Delay Compensation Based on Current Deviation in FCS-MPCC for Reduced THD and Torque Ripple in Surface-Mounted PMSM Drives

Thanh Quy Bach
Faculty of Electrical Engineering Technology, Industrial University of Ho Chi Minh City, Ho Chi Minh City, Vietnam
bachthanhquy@iuh.edu.vn (corresponding author)

Nhi Van Thi Kieu
Faculty of Electrical Engineering Technology, Industrial University of Ho Chi Minh City, Ho Chi Minh City, Vietnam
vanthikieunhi@iuh.edu.vn

Dai Le Van
Faculty of Electrical Engineering Technology, Industrial University of Ho Chi Minh City, Ho Chi Minh City, Vietnam
levandai@iuh.edu.vn

Received: 19 January 2026 | Revised: 5 March 2026 | Accepted: 15 March 2026

 DOI: https://doi.org/10.48084/etasr.17634

ABSTRACT

This paper proposes a delay-aware Finite Control Set Model Predictive Current Control (FCS-MPCC) for surface-mounted Permanent Magnet Synchronous Motor (PMSM) drives. The computation and actuation latency cause the measured current used for prediction to deviate from the actual regulated current at the switching moment, thereby impairing voltage-vector selection and elevating harmonics. To resolve this issue, the delay time is assessed, and the current deviation is reconstructed using the discrete PMSM model. The reconstructed current is then utilized as the initial state for prediction in each sampling interval. Comparative simulations of a 1.5 kW two-level inverter-fed PMSM drive demonstrate that the proposed method decreases stator-current THD from 14.2% (SS-MPCC) and 9.9% (DS-MPCC) to 7.3%. It also reduces torque ripple from 6.5 Nm and 4.4 Nm to 2.4 Nm, respectively, while enhancing transient and speed-reversal performance.

Keywords-model predictive current control; permanent magnet synchronous motor; compensation; time delay; torque ripple

I. INTRODUCTION

Permanent Magnet Synchronous Motors (PMSMs) are utilized in industrial drive systems due to their compact dimensions, elevated power density, superior efficiency, and low rotor inertia [1, 2]. Common applications encompass electric vehicles and servo drives [3], which necessitate low current harmonics, precise steady-state tracking, and rapid transient response.

Model Predictive Control (MPC) has attracted interest for PMSM drives because of its rapid dynamics, straightforward control architecture, and ability to handle constraints [4-6]. During each sampling interval, the controller assesses the potential inverter voltage options using a discrete prediction model and a cost function that measures the tracking error; the voltage-vector that minimizes the cost is subsequently implemented in the following control cycle.

Predictive control for PMSM drives has been formulated in various modalities, including Model Predictive Flux Control (MPFC) [7, 8], Model Predictive Speed Control (MPSC) [9, 10], Model Predictive Torque Control (MPTC) [11, 12], and Model Predictive Current Control (MPCC) [13, 14]. Among them, MPCC is utilized to optimize current tracking, diminish torque ripples, and augment transient performance.

In Finite Control Set Model Predictive Current Control (FCS-MPCC) [15, 16], the controller predicts the stator current at the next sampling instant using the measured current, the PMSM model, and the discrete voltage-vectors of the Voltage Source Inverter (VSI). The cost function is computed for each candidate vector, and the optimal switching state that yields the minimum current-tracking error is applied in the following cycle, providing fast response and accurate current regulation.

However, FCS-MPCC necessitates online calculation, resulting in a temporal delay between current measurement, prediction, and VSI actuation. Consequently, the current employed for initializing predictions may diverge from the actual regulated current, resulting in the selection of an inefficient switching state, heightened current harmonics, and torque ripple.

To address this issue, double-step MPCC forecasts over two sample periods, whereas alternative methods adjust for delay according to sampling principles [17, 18]. Alternative methods offer delay compensation based on sampling principles [19, 20]. While effective, these methods are either unsuitable for all situations or exacerbate computing demands. Consequently, improved delay compensation for MPCC remains necessary to optimize PMSM performance.

This paper proposes a precise model of predictive current control with delay compensation. The delay from the start of the current prediction to the selected voltage-vector execution is analyzed, and the deviation between the measured current and the actual controlled current is estimated from the PMSM model. The resulting compensated current is then used as the initial state of the prediction, enabling more reliable optimal voltage-vector selection. The performance is evaluated using transient indices and harmonic/torque metrics to quantify both dynamic and steady-state improvements [21]. The main contributions of this work are:

1. An in-depth examination of control-loop delay that clarifies the source of the prediction-measurement mismatch and its influence on VSI switching decisions.
2. A framework for delay-time computation and an associated current compensation formulation derived from the PMSM model, along with the proposed delay-compensation system.
3. Integration of the delay-compensated current into the MPCC cost function to determine the optimal control voltage vector in the following control cycle.
4. Comprehensive simulation comparisons that illustrate enhanced steady-state and dynamic performance of PMSM drives utilizing the proposed technique.

II. THEORETICAL BACKGROUND

A. Voltage Source Inverter

A two-level three-phase VSI supplies the PMSM, as shown in Figure 1(a). The VSI consists of a DC link and six power semiconductor switches and generates a finite set of stator voltage-vectors required for PMSM drives [22].

It produces six active and two zero voltage space vectors corresponding to the switching states $S_a, S_b, S_c, \overline{S_a}, \overline{S_b}, \overline{S_c}$ as illustrated in the space-vector diagram in Figure 1(b). This finite voltage-vector set forms the basis of FCS-MPCC, where all candidate vectors can be evaluated online during each sampling period. For clarity, $S_x \in \{0,1\}$ indicates the lower/upper switch state of phase $x \in \{a, b, c\}$.

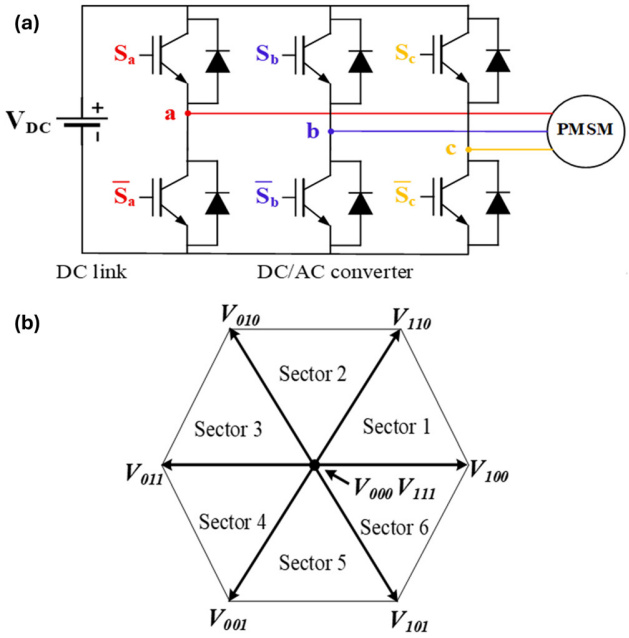

Fig. 1. The two-level VSI: (a) VSI topology for PMSM and (b) output voltage-vectors generated by the VSI.

The dq-axis components of the inverter output voltage-vector, obtained from the switching states and the electrical angle θ_e, can be written as:

$$\begin{bmatrix} u_d \\ u_q \end{bmatrix} = \frac{2}{3} V_{dc} \cdot \begin{bmatrix} cos\theta_e & cos\left(\theta_e - \frac{2\pi}{3}\right) & cos\left(\theta_e + \frac{2\pi}{3}\right) \\ -sin\theta_e & -sin\left(\theta_e - \frac{2\pi}{3}\right) & -sin\left(\theta_e + \frac{2\pi}{3}\right) \end{bmatrix} \begin{bmatrix} S_a \\ S_b \\ S_c \end{bmatrix} \quad (1)$$

where u_d and u_q denote the stator voltages in the dq-axis, θ_e is the electrical angular position, and V_{dc} is the voltage supplying the VSI.

B. PMSM Mathematical Model

The PMSM electrical dynamics in the rotating dq reference frame are described by:

$$\begin{cases} \frac{di_d}{dt} = -\frac{R_s}{L_d} i_d + \omega_e \frac{L_q}{L_d} i_q + \frac{1}{L_d} u_d \\ \frac{di_q}{dt} = -\frac{R_s}{L_q} i_q - \omega_e \frac{L_d}{L_q} i_d + \frac{1}{L_q} u_q - \omega_e \frac{\varphi_f}{L_q} \end{cases} \quad (2)$$

where i_d and i_q are the stator currents, R_s is the stator resistance, L_d and L_q are the dq-axis inductances, ω_e is the electrical angular speed, and φ_f is the permanent-magnet flux linkage.

The electromagnetic torque is given by (3). For a Surface-mounted PMSM (SPMSM), $L_d \approx L_q$, and the torque is mainly governed by i_q; therefore, improving current tracking in the q-axis directly reduces torque ripple [23].

$$T_e = \frac{3}{2}p\left[\varphi_d i_q - \varphi_q i_d\right] \quad (3)$$

where p is the pole pairs, and φ_d, φ_q are the stator flux components along the dq-axis.

The torque equilibrium equation on the motor shaft is given by:

$$T_e - T_L = J\frac{d\omega_m}{dt} + B_m\omega_m \quad (4)$$

where the load torque is T_L, J and B_m are the moment of inertia and the friction coefficient of the rotor, respectively, ω_m denotes the mechanical angular speed of the rotor, and $\omega_e = p\omega_m$.

C. The Single-Step MPCC (SS-MPCC)

According to [24], in MPCC using the Euler approximation, the discrete dq-axis currents are predicted as:

$$\begin{aligned} i_{dp}(k+1) &= \left(1-\frac{R_sT_s}{L_d}\right)i_{dm}(k) + \omega_e(k)\frac{L_qT_s}{L_d}i_{qm}(k) \\ &\quad + \frac{T_s}{L_d}u_d(k) \\ i_{qp}(k+1) &= -\omega_e(k)\frac{L_dT_s}{L_q}i_{dm}(k) + \left(1-\frac{R_sT_s}{L_q}\right)i_{qm}(k) \\ &\quad + \frac{T_s}{L_q}u_q(k) - \omega_e(k)\frac{\varphi_fT_s}{L_q} \end{aligned} \quad (5)$$

where k is the present instant, $i_{dm}(k)$ and $i_{qm}(k)$ are the stator measured currents at k^{th} instant, T_s is the sampling period, and $i_{dp}(k+1)$ and $i_{qp}(k+1)$ represent the dq -axis predictive currents at the next instant.

The single-step MPCC for PMSM drives based on the cost function evaluates the tracking error between the predictive currents and the reference currents [25]:

$$O_1 = \left(i_d^* - i_{dp}(k+1)\right)^2 + \left(i_q^* - i_{qp}(k+1)\right)^2 \quad (6)$$

At each sampling period, the cost function is computed for all candidate voltage-vectors, and the vector that minimizes the objective function is applied in the next cycle (Figure 2(a)).

Accordingly, SS-MPCC regulates the stator current in the following cycle, improving steady-state current quality and torque behavior.

D. The Double Step MPCC (DS-MPCC)

Double step MPCC is introduced to reduce the mismatch between the measured current used for prediction and the actual controlled current caused by computation delay.

As depicted in Figure 2(b), the voltage-vector computed at t_k is applied during the part of the $(k+1)^{th}$ and the initial part of $(k+2)^{th}$ cycle, so the one-step optimal choice may become suboptimal. Therefore, DS-MPCC selects the voltage-vector by considering current tracking over two future sampling instants.

The two-step MPCC is described in [18]. $i_{dp}(k+2)$ and $i_{qp}(k+2)$ are the predicted currents at the $(k+2)^{th}$ instant, as shown in:

$$\begin{cases} i_{dp}(k+2) = \left(1-\frac{R_sT_s}{L_d}\right)i_{dp}(k+1) + \\ \omega_e(k+1)\frac{L_qT_s}{L_d}i_{qp}(k+1) + \frac{T_s}{L_d}u_d(k+1) \\ i_{qp}(k+2) = -\omega_e(k+1)\frac{L_dT_s}{L_q}i_{dp}(k+1) + \\ \left(1-\frac{R_sT_s}{L_q}\right)i_{qp}(k+1) + \frac{T_s}{L_q}u_q(k+1) - \omega_e(k+1)\frac{\varphi_fT_s}{L_q} \end{cases} \quad (7)$$

The predictive voltages at $(k+1)^{th}$ instant are given by:

$$\begin{bmatrix} u_d(k+1) \\ u_q(k+1) \end{bmatrix} = \frac{2}{3}V_{dc}.M.\begin{bmatrix} S_a \\ S_b \\ S_c \end{bmatrix} \quad (8)$$

where:

$$M = \begin{bmatrix} cos\theta_e(k+1) & \cos\left(\theta_e(k+1)-\frac{2\pi}{3}\right) & \cos\left(\theta_e(k+1)+\frac{2\pi}{3}\right) \\ -sin\theta_e(k+1) & -sin\left(\theta_e(k+1)-\frac{2\pi}{3}\right) & -sin\left(\theta_e(k+1)+\frac{2\pi}{3}\right) \end{bmatrix} \quad (9)$$

Because the rotor inertia is large, the electrical angular speed can be assumed to be constant over one step, $\omega_e(k+1) \approx \omega_e(k)$. The predicted electrical angle is given by:

$$\theta_e(k+1) = \theta_e(k) + \omega_e(k).T_s \quad (10)$$

The objective functions of the double step MPC of PMSM are described using [26]:

$$\begin{aligned} O_2 &= \left[\left(i_d^* - i_{dp}(k+1)\right)^2 + \left(i_{qp}^* - i_{qp}(k+1)\right)^2\right] \\ &\quad + \left[\left(i_d^* - i_{dp}(k+2)\right)^2 + \left(i_{qp}^* - i_{qp}(k+2)\right)^2\right] \end{aligned} \quad (11)$$

Equation (11) is evaluated for the eight voltage vectors, and the vector that yields the minimum cost is applied in the next sampling period.

III. PROPOSED CURRENT DELAY COMPENSATION MPCC TECHNIQUE (DCC-MPCC)

The proposed DCC-MPCC adjusts the initial current used in prediction to match the actual controlled current, ensuring that the optimal voltage-vector for the next control cycle is selected through the minimum objective function. This section analyzes the computation delay in MPCC and derives a current compensation method, followed by the control diagram and implementation flowchart.

A. Delay Time Analysis and Current Compensation

Figure 3 illustrates the principle of the proposed delay-compensated MPCC. First, the delay time TDT-DTD between the current sampling and the execution of the newly selected voltage-vector is estimated. Then, the measured current is compensated before being used to initialize the prediction. The delay is assumed constant within one sampling period, and the current variation over the short interval is approximated as linear.

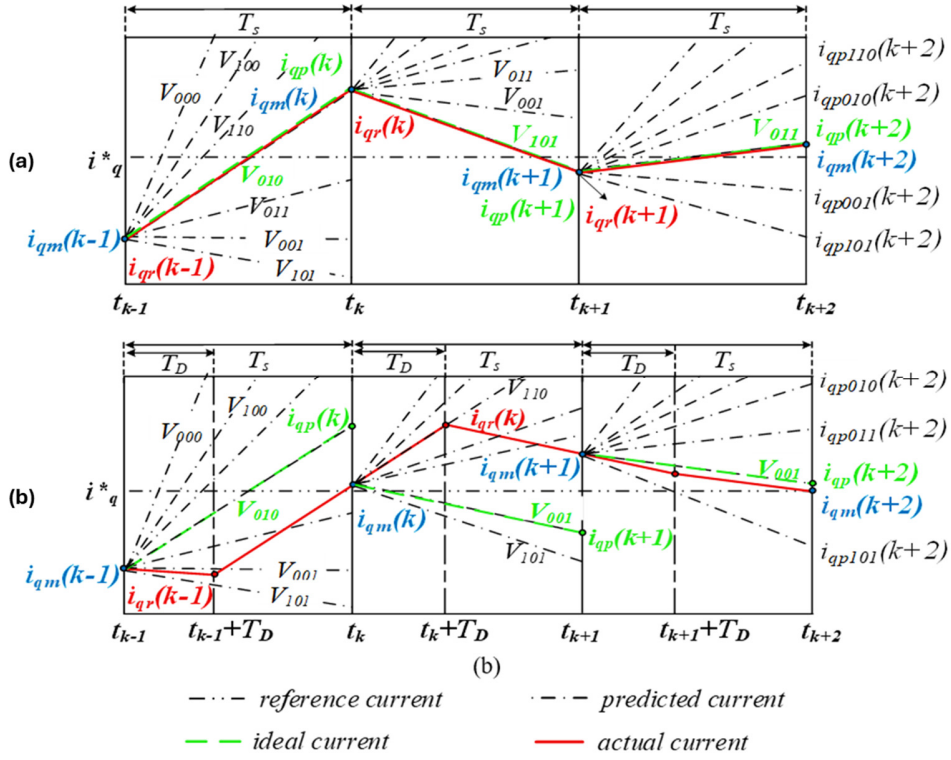

Fig. 2. MPCC's current trajectory: (a) ideal current of SS-MPCC and (b) actual current of SS-MPCC.

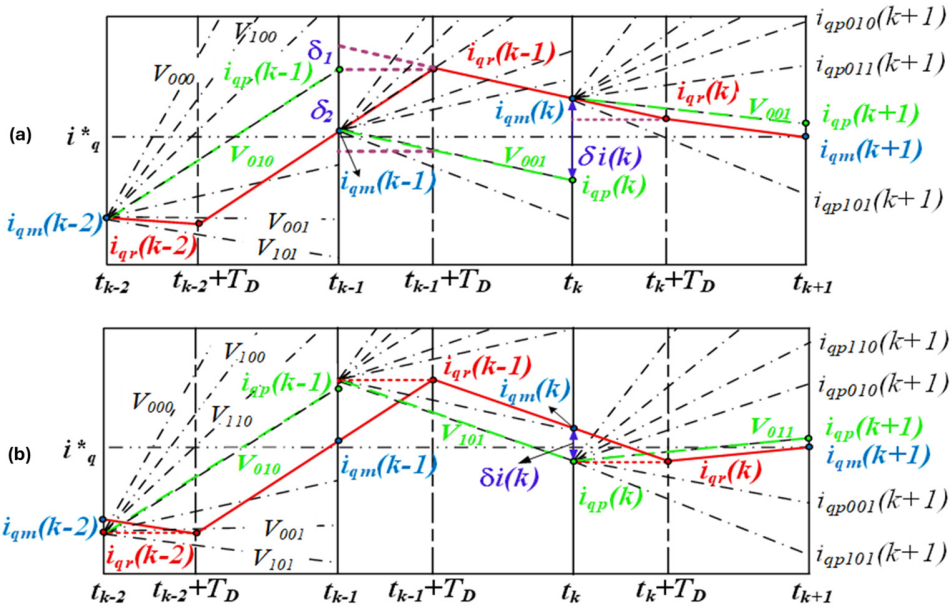

Fig. 3. Proposed DCC-MPCC implementation: (a) delay calculation and (b) delay current compensation.

As shown in Figure 3(a), the prediction computation introduces a delay time T_D in applying the selected voltage-vector. Therefore, the previous switching state remains active during the next control cycle; so, the measured current differs from the actual controlled current. The resulting prediction measurement mismatch is expressed by (12)-(13), where δ_1 and δ_2 represent the current variations associated with the $(k-1)^{\text{th}}$ and $(k-2)^{\text{th}}$ intervals, respectively:

$$\delta i(k) = i_{qm}(k) - i_{qp}(k) \quad (12)$$

On the other hand, $\delta i(k)$ can be described as:

$$\delta i(k) = \delta_1 + \delta_2 \quad (13)$$

where δ_1, δ_2 denote the changes of the predictive and actual currents at the $(k-1)^{\text{th}}$ and the $(k-2)^{\text{th}}$ time, respectively. The δ_1 and δ_2 components are calculated as detailed in the zoomed areas in Figures 4(a) and 4(b):

$$\delta_1 = \frac{T_D}{T_s}[i_{qm}(k-1) - i_{qp}(k)] \quad (14)$$

$$\delta_2 = \frac{T_D}{T_s}[i_{qm}(k-2) - i_{qp}(k-1)] \quad (15)$$

Equations (14) and (15) compute δ_1 and δ_2 using the linear-variation assumption, which leads to the delay-time estimation in:

$$T_D = \frac{[i_{qm}(k) - i_{qp}(k)].T_S}{[i_{qm}(k-2) - i_{qp}(k-1)] + [i_{qm}(k-1) - i_{qp}(k)]} \quad (16)$$

The compensated current at time k is then obtained as shown in (17), and the compensated currents are used to initialize the prediction in (18) instead of directly utilizing the measured currents. This reduces prediction errors caused by computation delays and improves voltage-vector selection despite latency:

$$i_{qc}(k) = i_{qr}(k) = i_{qm}(k) - \delta_1 \quad (17)$$

The predictive dq-axis currents of the proposed MPCC are calculated as:

$$\begin{cases} i'_{dp} = \left(1 - \frac{R_s T_s}{L_d}\right) i_{dc}(k) + \omega_e(k) \frac{L_q T_s}{L_d} i_{qc}(k) + \frac{T_s}{L_d} u_d(k) \\ i'_{qp} = -\omega_e(k) \frac{L_d T_s}{L_q} i_{dc}(k) + \left(1 - \frac{R_s T_s}{L_q}\right) i_{qc}(k) \\ \qquad + \frac{T_s}{L_q} u_q(k) - \omega_e(k) \frac{\varphi_f T_s}{L_q} \end{cases} \quad (18)$$

B. Procedure of the Proposed DCC-MPCC Strategy

With the delay estimation and the current compensation scheme, the DCC-MPCC procedure at time k is:

- Convert the measured three-phase currents (i_a, i_b, i_c) into the dq-axis currents (i_d, i_q) using Park transformation.
- Estimate T_D and compute the compensated currents (i_{dc}, i_{qc}).
- Predict the next-step currents using the compensated currents and the Euler approximation.
- Evaluate the objective function for all candidate voltage-vectors and select the vector with the minimum cost to be applied in the next cycle.
- Apply the corresponding switching state to the VSI to drive the PMSM.

The above procedure is implemented by the control diagram and flowchart depicted in Figures 5 and 6. The proposed approach is evaluated using the MATLAB/Simulink model illustrated in Figure 7.

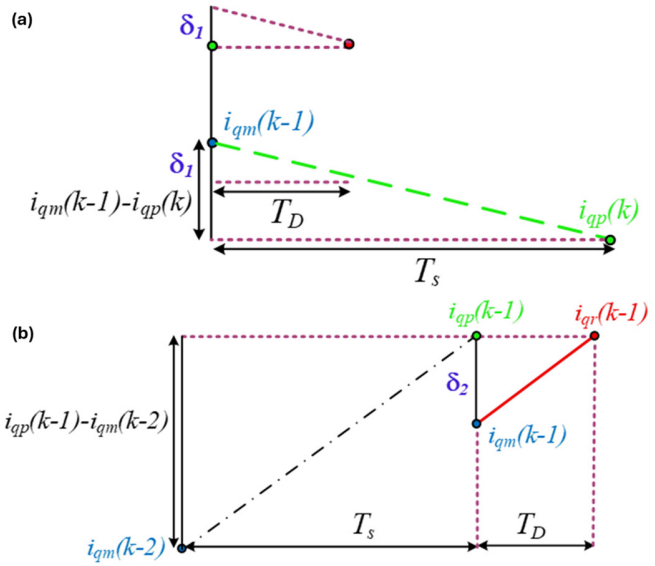

Fig. 4. Computing the difference between the predicted current and the actual current : (a) δ_1 component at $t_{(k-1)}$ and (b) δ_2 component at $t_{(k-2)}$.

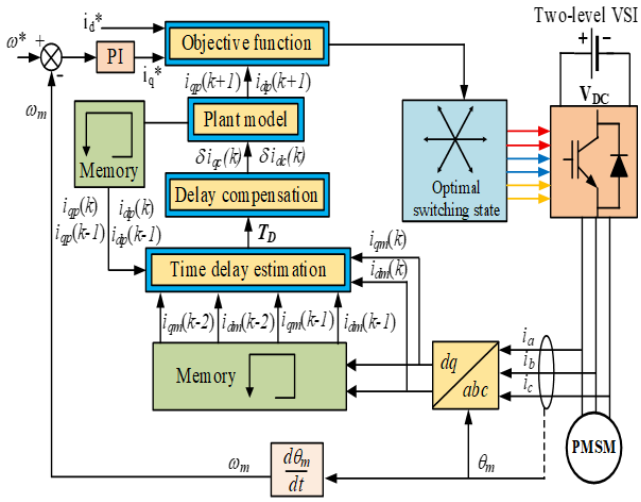

Fig. 5. Control diagram of the proposed DCC-MPCC algorithm.

IV. SIMULATION RESULTS AND ANALYSIS

This section benchmarks SS-MPCC, DS-MPCC, and the proposed DCC-MPCC using the same PMSM drive model and an identical operating profile to ensure a fair comparison. All controllers use the same PMSM/inverter parameters in Table I, the same reference signals, and the same candidate voltage-vector set; the only difference lies in how the prediction is initialized in the presence of computation/actuation delay.

The test profile is as follows: the motor accelerates from standstill to 94 rad/s under a 15 Nm load, the load steps to 20 Nm at 0.2 s and to 5 Nm at 0.25 s, the speed command drops to 30 rad/s at 0.35 s, and the motor reverses at 0.45 s. Performance is evaluated in terms of speed/torque transient indices, phase and dq-axis current quality, torque ripple, current THD, and computational burden.

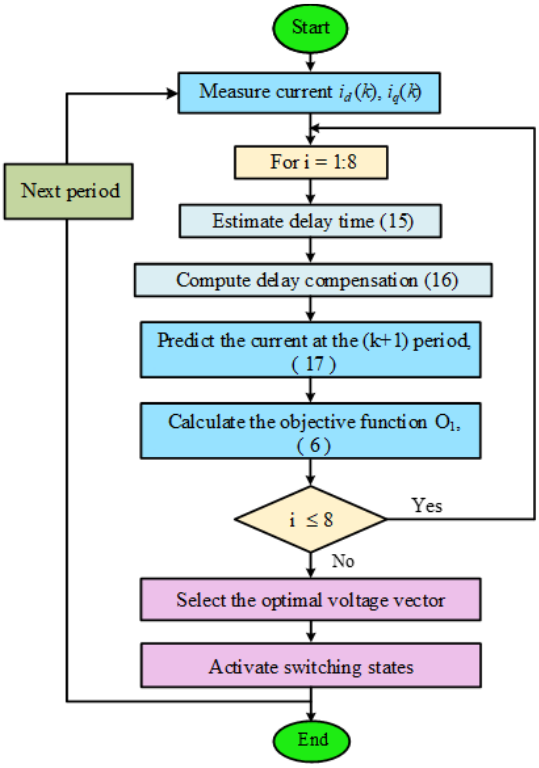

Fig. 6. Flowchart of the proposed DCC-MPCC algorithm.

TABLE I. PMSM DRIVE SYSTEM PARAMETERS

Parameters	Symbol	Value	Unit
Rated speed	n_r	900	rpm
Rated power	P_r	1.5	kW
Rated Torque	T_r	16	Nm
Pole pairs	p	4	
d-axis inductance	L_d	0.00097	H
q-axis inductance	L_q	0.00097	H
Stator resistance	R_s	0.11	Ω
Permanent magnet flux linkage	φ_f	0.1119	Wb
Viscous friction	B_m	0.0002024	N·m·s
DC-link voltage	U_{dc}	460	V
Total inertia	J	0.0016	kg·m^2

A. Comparative Analysis under the Transient Condition

For the transient comparison in Figure 8, four scenarios are considered: start-up, overload at 0.2 s, underload at 0.25 s, and deceleration to 30 rad/s at 0.35 s. Speed, torque, and phase current responses are compared. In Figure 8, all methods track the reference speed with similar steady-state accuracy, but slight differences appear during start-up, and the speed drops at 0.35 s. During start-up (in zoom-in 1), SS-MPCC reaches 115 rad/s and dips to 88 rad/s, DS-MPCC reaches 113 rad/s and dips to 89 rad/s, whereas DCC-MPCC shows the smallest deviation (110 rad/s max, 92 rad/s min). When the reference speed decreases to 30 rad/s at 0.35 s, the minimum speed drops to 7.7 rad/s (SS-MPCC), 9.2 rad/s (DS-MPCC), and 11.9 rad/s (DCC-MPCC) in the zoomed view, indicating that DCC-MPCC limits the speed dip more effectively. Table II summarizes the OS (overshoot), US (undershoot), and PS (preshoot) indices.

TABLE II. PMSM SPEED RESPONSE

Methods	Start-up			Decelerating at 0.35 s	
	OS (%)	US (%)	PS (%)	US (%)	PS (%)
SS-MPCC	22.3	6.4	2.6	74	0.9
DS-MPCC	20.2	5.3	2.4	69	1.0
DCC-MPCC	17.0	2.1	2.1	60	0.7

TABLE III. PMSM TORQUE PRESHOOT (%)

Methods	Starting up	Overload change at 0.2 s	Underload change at 0.25 s
SS-MPCC	26	64	26
DS-MPCC	20	40	17
DCC-MPCC	13	26	13

Torque tracking, as presented in Figure 8, confirms that all controllers meet the demanded torque, but DCC-MPCC reduces torque fluctuation in both transient and steady-state operation. Table III shows that DCC-MPCC yields the smallest torque preshoot during acceleration, load increase (0.2 s), and load decrease (0.25 s). The starting torque values are 33.7 Nm for SS-MPCC and DS-MPCC, and 32.8 Nm for DCC-MPCC (in zoom-in 3). During the sudden deceleration at 0.35 s (in zoom-in 4), the undershoot torques are −19.4 Nm (SS-MPCC), −17.4 Nm (DS-MPCC), and −17.3 Nm (DCC-MPCC). The reduced oscillation after load steps further indicates the advantage of DCC-MPCC for fast and stable PMSM drives.

Phase current waveforms are similar across methods, but DCC-MPCC slightly reduces peak currents during transients. The start-up current is 48.8 A for DCC-MPCC compared to 50.2 A for SS-MPCC/DS-MPCC (in zoom-in 5). Under overload, the phase currents are 34 A (SS-MPCC), 33 A (DS-MPCC), and 32 A (DCC-MPCC). When the load is reduced (in zoom-in 6), the current overshoot values are 27 A, 24.4 A, and 21.2 A, respectively.

Overall, DCC-MPCC reduces key transient indices (overshoot, undershoot, and preshoot) of speed, torque, and phase current compared to SS-MPCC and DS-MPCC.

B. Comparative Analysis under the Steady-State Condition

Under steady-state (94 rad/s, 15 Nm), the three methods are compared using the indicators provided in Figures 9-11. Figure 9 demonstrates that DCC-MPCC achieves the best current quality. SS-MPCC exhibits distorted phase currents (−26.1 A-25.8 A) with a THD of 14.2%, DS-MPCC improves THD to 9.9% (−25.6 A-25.2 A), whereas DCC-MPCC produces nearly sinusoidal currents (±24 A) with a THD of 7.3%. The spectra confirm that the proposed method suppresses harmonics more effectively. Figures 10 and 11 indicate that improved current tracking directly reduces torque ripples. The *dq*-axis current amplitudes are about 10 A (SS-MPCC), 6.6 A (DS-MPCC), and 3.8 A (DCC-MPCC). Accordingly, the torque ripple amplitudes are 6.5 Nm (SS-MPCC), 4.4 Nm (DS-MPCC; 32% lower than that of SS-MPCC), and 2.4 Nm (DCC-MPCC; 63% lower than that of SS-MPCC and 46% lower than that of DS-MPCC). DCC-MPCC also keeps torque closer to the 15 Nm reference.

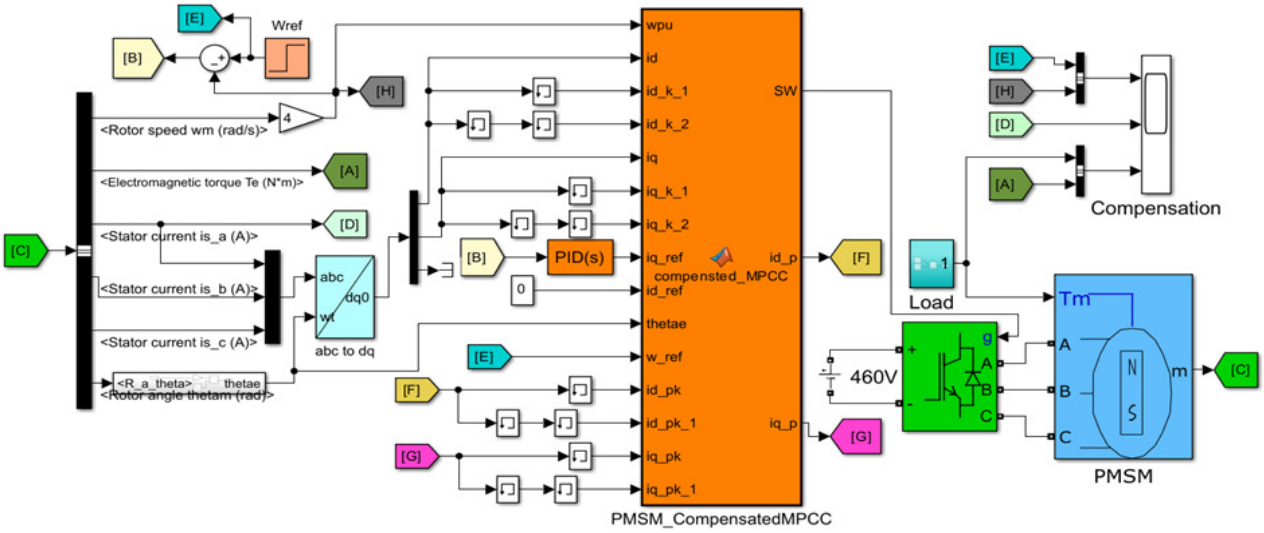

Fig. 7. Tested Simulink simulation of the proposed DCC-MPCC algorithm.

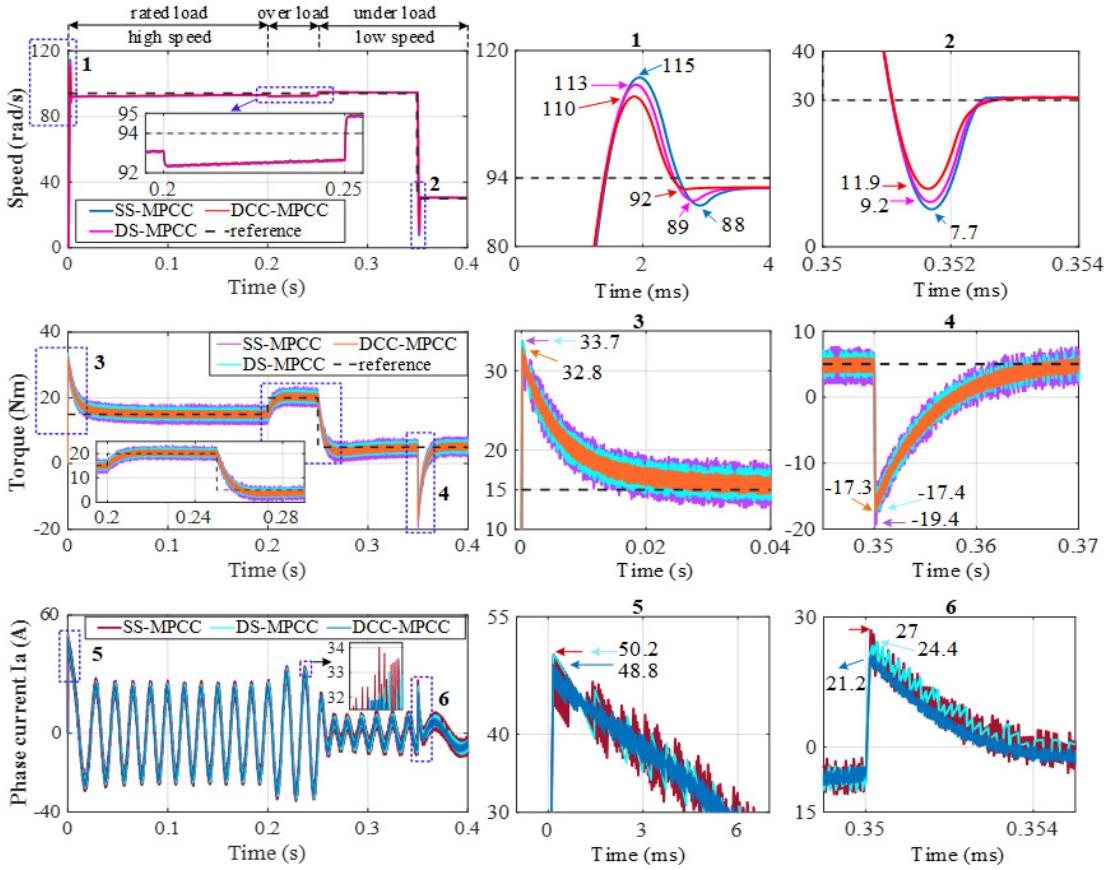

Fig. 8. Comparative results of three different control strategies under the transient condition.

These steady-state results confirm that delay compensation in MPCC significantly reduces the current THD and electromagnetic torque ripples, yielding the most stable response among the three strategies.

C. Comparative Analysis under the Reversal Condition

During reversal, the motor operates at 30 rad/s with a 5 Nm load, then reverses at 0.45 s and settles at a reverse speed of 40 rad/s. Figure 12 compares speed, torque, and phase current responses during this transition.

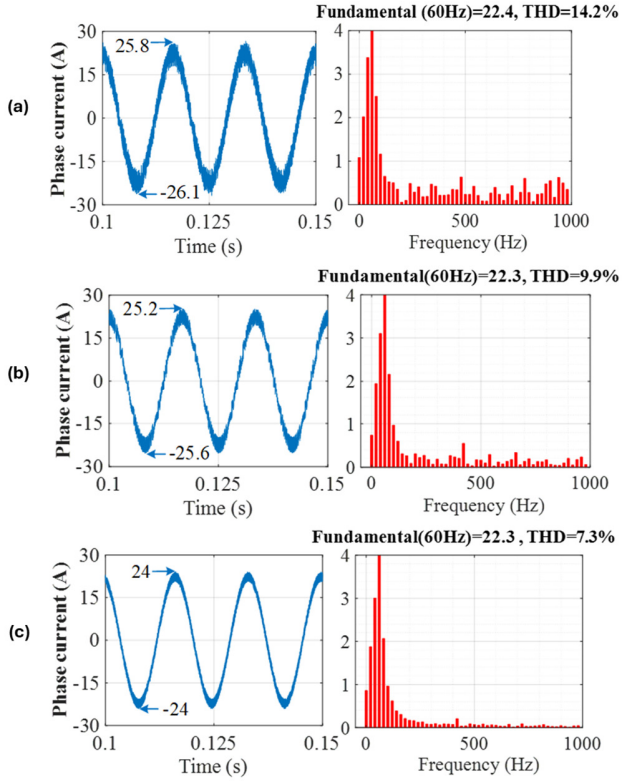

Fig. 9. Phase currents and current THD performances for the three different control strategies: (a) SS-MPCC, (b) DS-MPCC, and (c) DCC-MPCC.

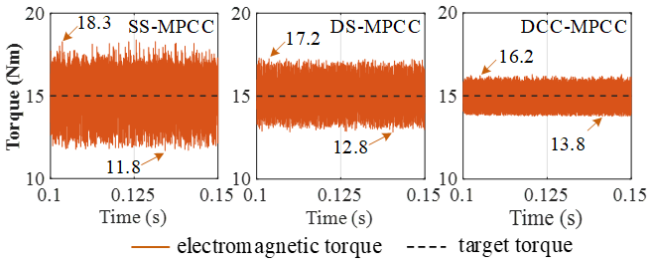

Fig. 10. Electromagnetic torque responses under the three different control strategies.

In Figure 12(a), all control methods complete reversal quickly, but DCC-MPCC shows the smallest speed deviation. During 0.451-0.453 s, SS-MPCC and DS-MPCC undershoot to approximately −58 rad/s and −56 rad/s, whereas DCC-MPCC limits it to −53 rad/s, indicating smoother low-speed reversal.

Figure 12(b) shows that DCC-MPCC improves torque tracking during reversal, with a smaller undershoot of −19 Nm compared to −20.2 Nm (SS-MPCC) and −20 Nm (DS-MPCC). In Figure 12(c), the peak phase current is 27 A for DCC-MPCC compared to 29 A for SS-MPCC and DS-MPCC.

Therefore, DCC-MPCC provides slightly better speed, torque, and current behavior under reversal operation.

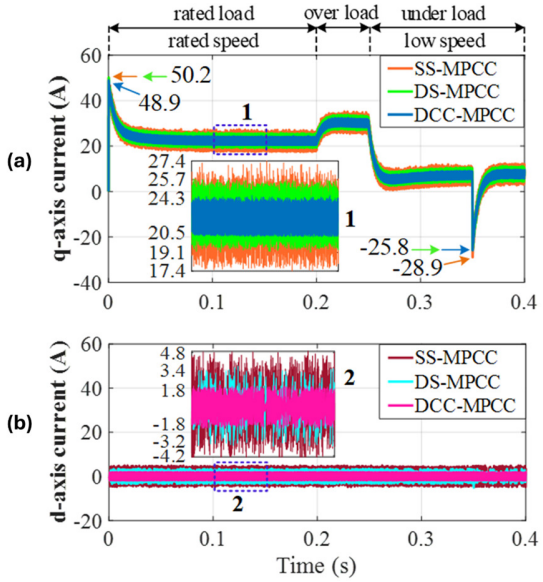

Fig. 11. Current performance of the three control strategies: (a) q-axis current component and (b) d-axis current component.

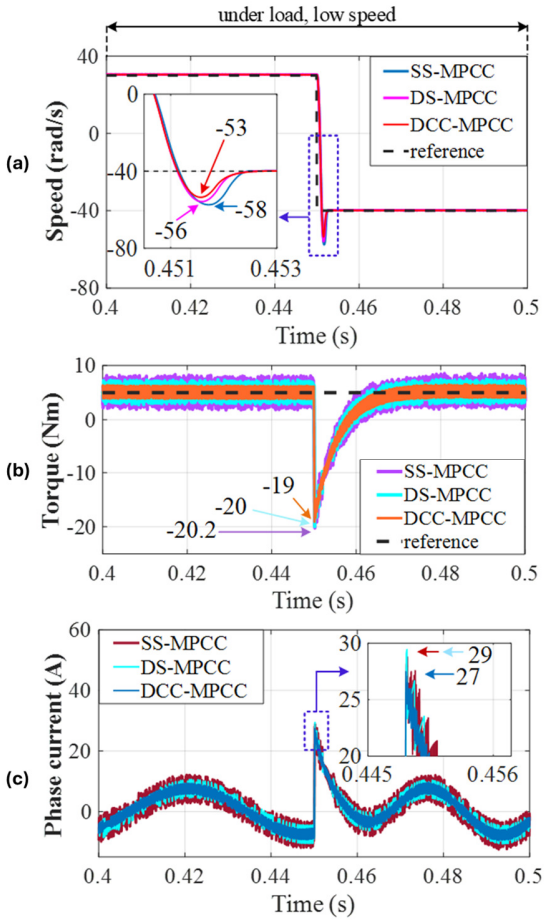

Fig. 12. Comparative results under reversal conditions: (a) speed, (b) electromagnetic torque, and (c) phase current performances.

D. Sensitivity Analysis

This sensitivity analysis compares torque control quality. Specifically, the performance is evaluated using torque errors, namely Integral Time Absolute Error (ITAE), Integral Absolute Error (IAE), and Integral Square Error (ISE), and computational burden metrics (self-time, execution time per step, and operation count), as displayed in Figure 13.

The evaluation indicators IAE, ITAE, and ISE are determined using:

$$IAE = \int_0^t |e(t)|dt \quad (19)$$

$$ITAE = \int_0^t |e(t)|tdt \quad (20)$$

$$ISE = \int_0^t e^2(t)dt \quad (21)$$

In Figure 13(a), DCC-MPCC yields the smallest torque-error indices (IAE=0.7, ITAE=0.2, ISE=4.6), whereas SS-MPCC shows the largest errors (IAE=1.1, ITAE=0.4, ISE=5.6), and DS-MPCC provides intermediate performance.

According to Figure 13(b), SS-MPCC has the lowest self-time (2 s) and call number (600,000), indicating the lightest online computational load. DS-MPCC requires slightly more resources (2.1 s; 1,200,000), and DCC-MPCC has the highest burden (7.2 s; 3,500,000). The execution time per step of DCC-MPCC is 2 µs, slightly longer than that of DS-MPCC (1.8 µs), but still faster than that of SS-MPCC.

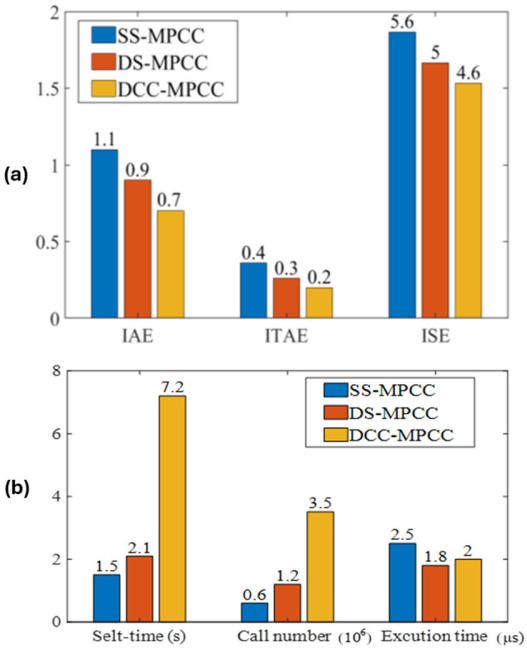

Fig. 13. Trade-offs between computational burden and control algorithm efficiency of the three strategies: (a) torque errors and (b) computing time.

Overall, the analysis demonstrates a clear trade-off: SS-MPCC is the most computationally efficient technique, whereas DCC-MPCC prioritizes performance at the expense of higher computational cost, with DS-MPCC serving as an intermediate compromise between the two. Future research aims to reduce the computational complexity associated with predictive modeling algorithms.

The key metrics are outlined in Table IV.

TABLE IV. KEY METRICS

Parameters	SS-MPCC	DS-MPCC	DCC-MPCC
Execution time per step (µs)	2.5	1.8	2
Current THD (%)	14.2	9.9	7.3
Iq deviation (A)	10	6.6	3.8
Id deviation (A)	10	6.6	3.8
Electromagnetic torque fluctuating amplitude (Nm)	6.5	4.4	2.4
IAE	1.1	0.9	0.7
ITAE	0.4	0.3	0.2
ISE	5.6	5	4.6

V. CONCLUSIONS

This work introduced a delay-compensated Finite Control Set Model Predictive Current Control (FCS-MPCC) for Permanent Magnet Synchronous Motor (PMSM) drives. The proposed method rectifies the initial state prediction and enhances voltage-vector selection under latency by calculating computation/actuation delay and reconstructing the current deviation. Simulation results validate reduced current harmonics and torque ripple (THD: 14.2%-7.3%; torque ripple: 6.5 Nm-2.4 Nm), alongside enhanced transient and speed-reversal responses. Future research will concentrate on: real-time embedded implementation (DSP/MCU/FPGA) with code-level optimization to minimize worst-case latency, high-speed/field-weakening validation utilizing constraint-aware multi-objective cost design (tracking–loss–thermal), and robustness improvements under parameter uncertainty through online identification and disturbance observers.

REFERENCES

[1] L. Guo, Y. Wang, H. Wang, and Z. Zhang, "Design of high power density double-stator permanent magnet synchronous motor," *IET Electric Power Applications*, vol. 17, no. 4, pp. 421–431, April 2023, https://doi.org/10.1049/elp2.12275.

[2] T.-L. Le and M.-F. Hsieh, "An enhanced direct torque control strategy with composite controller for permanent magnet synchronous motor," *Asian Journal of Control*, vol. 26, no. 4, pp. 1683–1702, July 2024, https://doi.org/10.1002/asjc.3306.

[3] K. Yang, H. Li, and S. Li, "Composite model predictive current control for PMSM servo system," *Transactions of the Institute of Measurement and Control*, 2025, Art. no. 01423312241295793, https://doi.org/10.1177/01423312241295793.

[4] Y. Liu *et al*., "Three-Vector-Based Model Predictive Torque Control for Dual Three-Phase PMSM With Torque and Flux Ripples Reduction," *IEEE Transactions on Power Electronics*, vol. 39, no. 8, pp. 10009–10020, Aug. 2024, https://doi.org/10.1109/TPEL.2024.3390791.

[5] Y. Wei, H. Young, D. Ke, F. Wang, and J. Rodríguez, "Model-Free Predictive Current Control Using Extended Affine Ultralocal for PMSM Drives," *IEEE Transactions on Industrial Electronics*, vol. 71, no. 7, pp. 6719–6729, July 2024, https://doi.org/10.1109/TIE.2023.3314914.

[6] H. Kawai, Z. Zhang, R. Kennel, and S. Doki, "Direct Speed Control Based on Finite Control Set Model Predictive Control With Voltage Smoother," *IEEE Transactions on Industrial Electronics*, vol. 70, no. 3, pp. 2363–2372, Mar. 2023, https://doi.org/10.1109/TIE.2022.3174298.

[7] Y. Xu, Y. Zhang, Q. Gao, and Z. Yin, "A Wide-Speed Range Three-Vector-Based Model Predictive Flux Control With Improved Predictive

Model for PMSM Drives," *IEEE Transactions on Transportation Electrification*, vol. 10, no. 2, pp. 2689–2700, June 2024, https://doi.org/10.1109/TTE.2023.3299652.

[8] X. Wu *et al*., "Parameter-Free Predictive Torque and Flux Control for PMSM Based on Incremental Stator Flux Predictive Model," *IEEE Transactions on Industrial Informatics*, vol. 20, no. 2, pp. 2715–2726, Feb. 2024, https://doi.org/10.1109/TII.2023.3295413.

[9] M. Yang *et al*., "Enhanced Model-Free Predictive Speed Control Without Weighting Factors for PMSM Based on Newly Designed Cost Function," *IEEE Transactions on Transportation Electrification*, vol. 10, no. 3, pp. 5703–5714, Sept. 2024, https://doi.org/10.1109/TTE.2023.3318736.

[10] A. R. Raut and S. V. Jadhav, "Model Predictive Speed Control of Permanent Magnet Synchronous Motor," in *2022 IEEE International Conference on Power Electronics, Drives and Energy Systems* (*PEDES*), Jaipur, India, Sept. 14–17, 2022, pp. 1–6, https://doi.org/10.1109/PEDES56012.2022.10080344.

[11] Z. Yang, C. Miao, X. Sun, and D. Guo, "Robust Model Predictive Torque Control of Interior PMSM Drives With Kalman-Based Disturbance Observer," *IEEE Transactions on Transportation Electrification*, vol. 10, no. 2, pp. 2434–2444, June 2024, https://doi.org/10.1109/TTE.2023.3296684.

[12] I. D. De Martin, A. Brosch, F. Tinazzi, and M. Zigliotto, "Continuous Control Set Model Predictive Torque Control With Minimum Current Magnitude Criterion for Synchronous Motor Drives," *IEEE Transactions on Industrial Electronics*, vol. 71, no. 7, pp. 6787–6796, July 2024, https://doi.org/10.1109/TIE.2023.3308132.

[13] M. A. Khamis, A. A. Ahmed, A. M. Omara, and E. E. M. Rashad, "Performance Enhancement of SPMSM Under Finite Control Set Model Predictive Current Control," in *24th International Middle East Power System Conference* (*MEPCON*), Mansoura, Egypt, Dec. 19–21, 2023, pp. 1–7, https://doi.org/10.1109/MEPCON58725.2023.10462407.

[14] M. L. Parvathy and V. K. Thippiripati, "A Simplified Voltage Vector Preselection-Based Multivector Predictive Current Control for Improved Torque Performance of PMSM Drive," *IEEE Transactions on Power Electronics*, vol. 38, no. 7, pp. 8775–8785, July 2023, https://doi.org/10.1109/TPEL.2023.3267107.

[15] T. Li, X. Sun, G. Lei, Y. Guo, Z. Yang, and J. Zhu, "Finite-Control-Set Model Predictive Control of Permanent Magnet Synchronous Motor Drive Systems—An Overview," *IEEE/CAA Journal of Automatica Sinica*, vol. 9, no. 12, pp. 2087–2105, Dec. 2022, https://doi.org/10.1109/JAS.2022.105851.

[16] J. Rodriguez *et al*., "Latest Advances of Model Predictive Control in Electrical Drives—Part I: Basic Concepts and Advanced Strategies," *IEEE Transactions on Power Electronics*, vol. 37, no. 4, pp. 3927–3942, Apr. 2022, https://doi.org/10.1109/TPEL.2021.3121532.

[17] L. Xu, Y. Deng, H. Li, C. Zhai, W. Li, and H. Cao, "Model Predictive Current Control of PMSM with Enhanced Robustness Against Parameter Mismatch," in *2025 IEEE International Conference on Predictive Control of Electrical Drives and Power Electronics* (*PRECEDE*), Nanjing, China, June 5–8, 2025, pp. 1–6, https://doi.org/10.1109/PRECEDE63178.2025.11130943.

[18] Y. Li, Z. Liu, T. Wu, R. Tong, X. Zhang, and Y. Deng, "Two-step Model-free Predictive Current Control for PMSM," in *2023 IEEE International Conference on Predictive Control of Electrical Drives and Power Electronics* (*PRECEDE*), Wuhan, China, June 16–19, 2023, pp. 1–6, https://doi.org/10.1109/PRECEDE57319.2023.10174584.

[19] C. Gong, L. Ding, Y. Li, and J. Li, "Improved Sensorless FCS-MPCC With Current Pre-Estimation-Based Delay Compensation Integrated for PMSMs Over High-Speed Range," *IEEE Transactions on Industry Applications*, vol. 59, no. 6, pp. 6756–6765, 2023, https://doi.org/10.1109/TIA.2023.3298307.

[20] C. Gong, L. Ding, Y. Li, and J. Li, "Current Pre-Estimation-based Delay Compensation for Sensorless FCS-MPCC Used in PMSM Drives Over High-Speed Range," in *25th International Conference on Electrical Machines and Systems* (*ICEMS*), Chiang Mai, Thailand, Nov. 29 – Dec. 2, 2022, pp. 1–5, https://doi.org/10.1109/ICEMS56177.2022.9982845.

[21] A. Balestrino, A. Landi, M. Medaglia, and M. Satler, "Performance Indices and Tuning in Process Control," in *14th Mediterranean Conference on Control and Automation*, Ancona, Italy, June 28–30, 2006, pp. 1–6, https://doi.org/10.1109/MED.2006.328852.

[22] S. S. P. Musti and R. Bhimasingu, "A Novel DC-link Midpoint Switching Scheme for Common-Mode Voltage Mitigation in 3-Phase 2-Level VSI," in *11th National Power Electronics Conference* (*NPEC*), Guwahati, India, Dec. 14–16, 2023, pp. 1–6, https://doi.org/10.1109/NPEC57805.2023.10384957.

[23] K. Cherif, A. Sahbani, and K. B. Saad, "Performance Evaluation of PI and Sliding Mode Control for PMSM in Applications for Electric Vehicles," *Engineering, Technology & Applied Science Research*, vol. 14, no. 4, pp. 15464–15470, Aug. 2024, https://doi.org/10.48084/etasr.7172.

[24] J. Hang, H. Wu, J. Zhang, S. Ding, Y. Huang, and W. Hua, "Cost Function-Based Open-Phase Fault Diagnosis for PMSM Drive System With Model Predictive Current Control," *IEEE Transactions on Power Electronics*, vol. 36, no. 3, pp. 2574–2583, Mar. 2021, https://doi.org/10.1109/TPEL.2020.3011450.

[25] X. Sun, M. Wu, G. Lei, Y. Guo, and J. Zhu, "An Improved Model Predictive Current Control for PMSM Drives Based on Current Track Circle," *IEEE Transactions on Industrial Electronics*, vol. 68, no. 5, pp. 3782–3793, May 2021, https://doi.org/10.1109/TIE.2020.2984433.

[26] X. Wang, H. Cao, H. Sun, and P. Wang, "Simplified Algorithm for Multi-Step Model Predictive Control of Permanent Magnet Synchronous Motors for Ship Propulsion," *IEEJ Transactions on Electrical and Electronic Engineering*, vol. 20, no. 8, pp. 1268–1281, Aug. 2025, https://doi.org/10.1002/tee.24278.